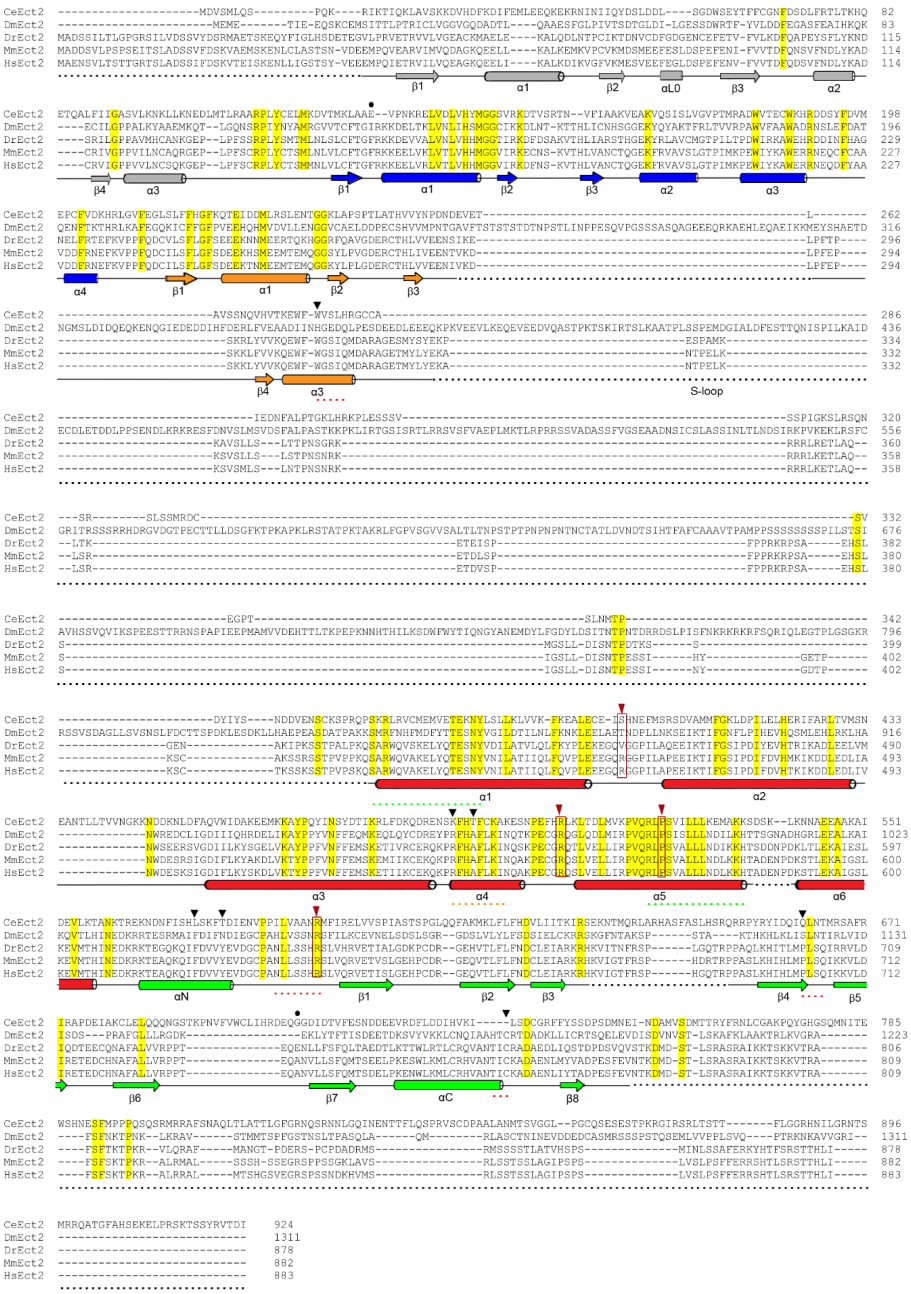

Fig. S1 Multiple sequence alignments of Ect2 homologs. Secondary structural assignments labeled at the bottom are based on the structure determined in this study except the BRCT0 (grey) based on previous structure (PDB code 4N40) (1). Residues involved in the autoinhibition interface, dotted lines (red, binding to the DH domain; orange, binding to the BRCT2 domain; green, binding to the PH domain) ; the conserved residues, highlighted in yellow; the residues mutated in this study, triangles (the cancer associated mutations in red); residues mutated leading to ECT-2 activation in *C. elegans* (2), black circles.

www.pnas.org/cgi/doi/10.1073/pnas.1913054117

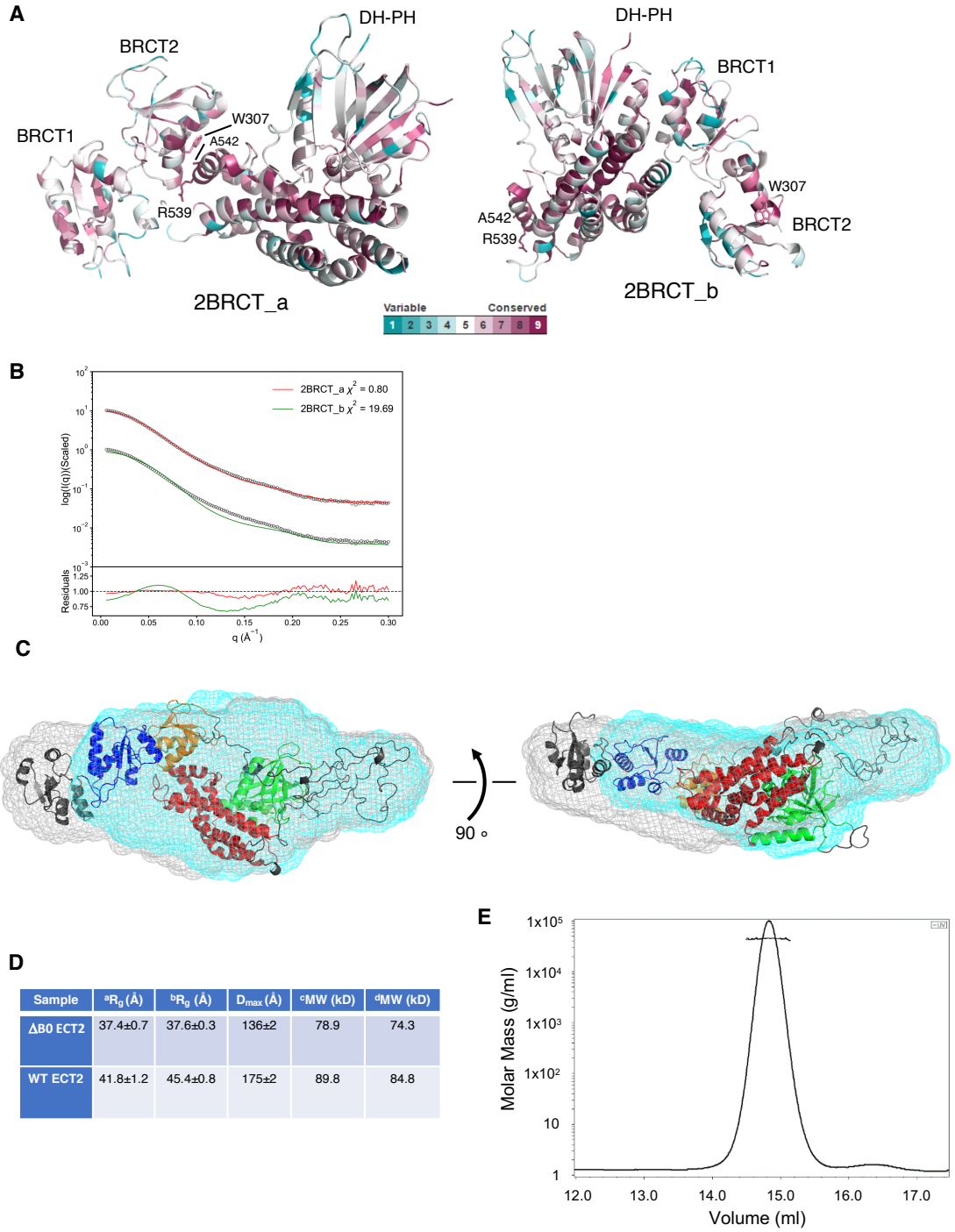

Sample	[a]R_g (Å)	[b]R_g (Å)	D_{max} (Å)	[c]MW (kD)	[d]MW (kD)
ΔB0 ECT2	37.4±0.7	37.6±0.3	136±2	78.9	74.3
WT ECT2	41.8±1.2	45.4±0.8	175±2	89.8	84.8

Fig. S2 SAXS and MALS analyses of Ect2. (**A**) Two possible crystal packing interactions of Ect2 (2BRCT_a and 2BRCT_b). Three residues (W307, R539, and A542) involved in the packing interface are shown as sticks. The conservation scores of the residues are color coded. (**B**) Top, overlays of the experimental scattering profile (black circles) and those back-calculated from the models of 2BRCT_a (red)

and 2BRCT_b (green). Bottom, residual differences in the scattering curves between the back-calculated and experimental ones. (**C**) Docking of the models of WT and ΔB0 Ect2 to the reconstructed molecular envelops based on the SAXS measurements. Molecular envelop of WT Ect2, grey; the one of ΔB0 Ect2, cyan. Missing residuals, including the discorded S-loop and the C-terminal tail, were added by the SWISS-model server (3) and colored dark grey. (**D**) Structural parameters of WT and ΔB0 Ect2. (**E**) MALS analysis of DP Ect2 (residues: 408-790). The measured molecular weight is 44 kDa, consistent with a monomer.

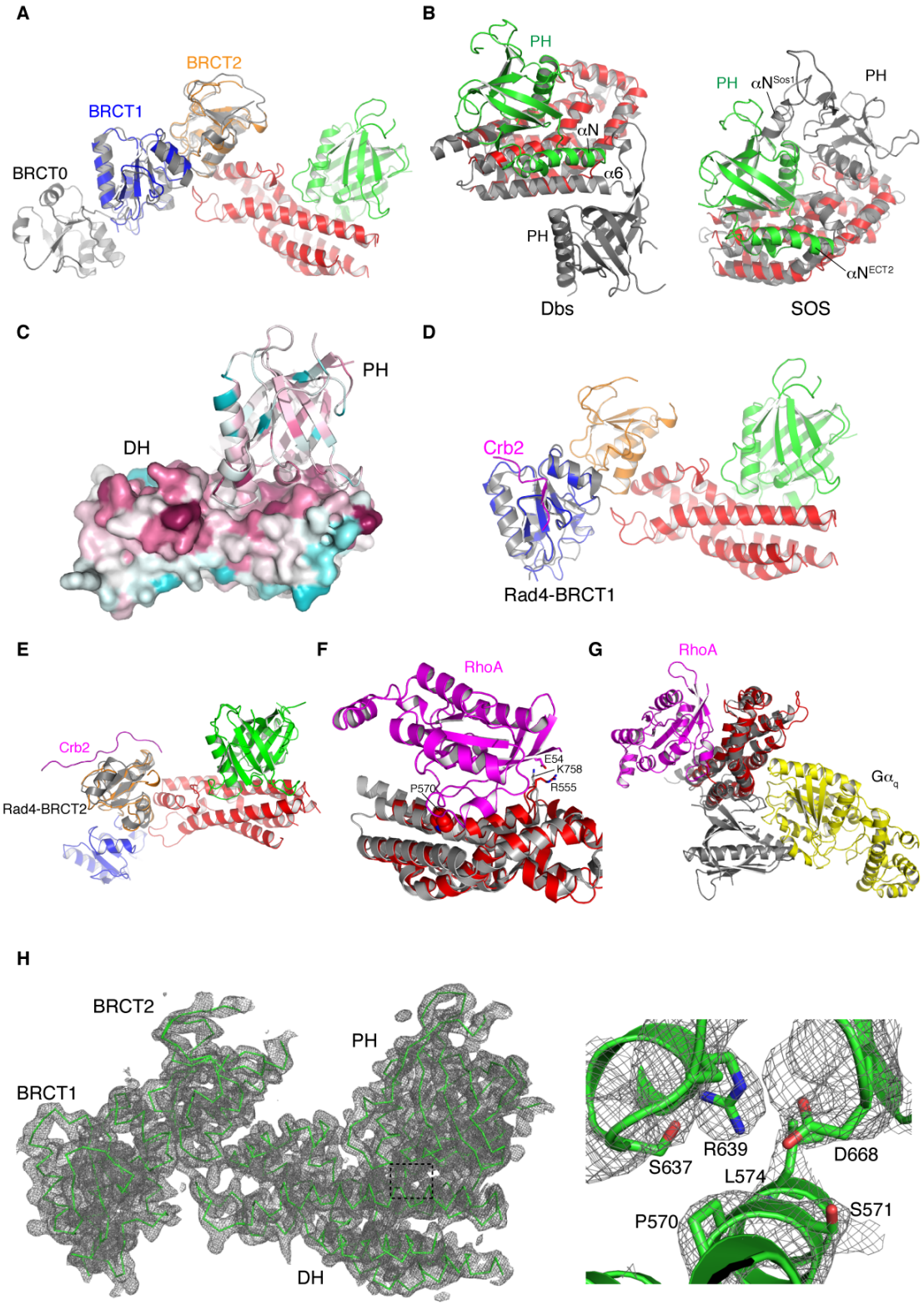

Fig. S3 Additional structural analysis of Ect2. (**A**) Comparison of the tandem BRCT domains. The structure determined in this study, color coded; the previous one (PDB code 4N40) (1), grey. (**B**) Structural alignments of the DH domains of Ect2 (color coded) with Dbs (left panel, grey, PDB code 1lb1)(4) and SOS (right panel,

grey, PDB code 1dbh)(5). (**C**) Surface conservation analysis. The conservation scores are calculated by The ConSurf Sever and color coded (6). (**D-E**) Superposition of the structures of the BRCT1 (D) and BRCT2 (E) of Ect2 with that of Rad4 bound to the phospho-Crb2 peptide (PDB code 4BU0) (7). (**F-G**) Structural alignments of the DH domain of Ect2 (red) with that of Dbs (F, grey, PDB code 1lb1) (4) and p63RhoGEF (G, grey, PDB code 2rgn)(8) bound to RhoA (magenta). The PH and BRCT domains of Ect2 are omitted for clarity. (**H**) 2Fo-Fc electron map of Ect2. The boxed region (around the Arg639 region) is enlarged for a close-up view.

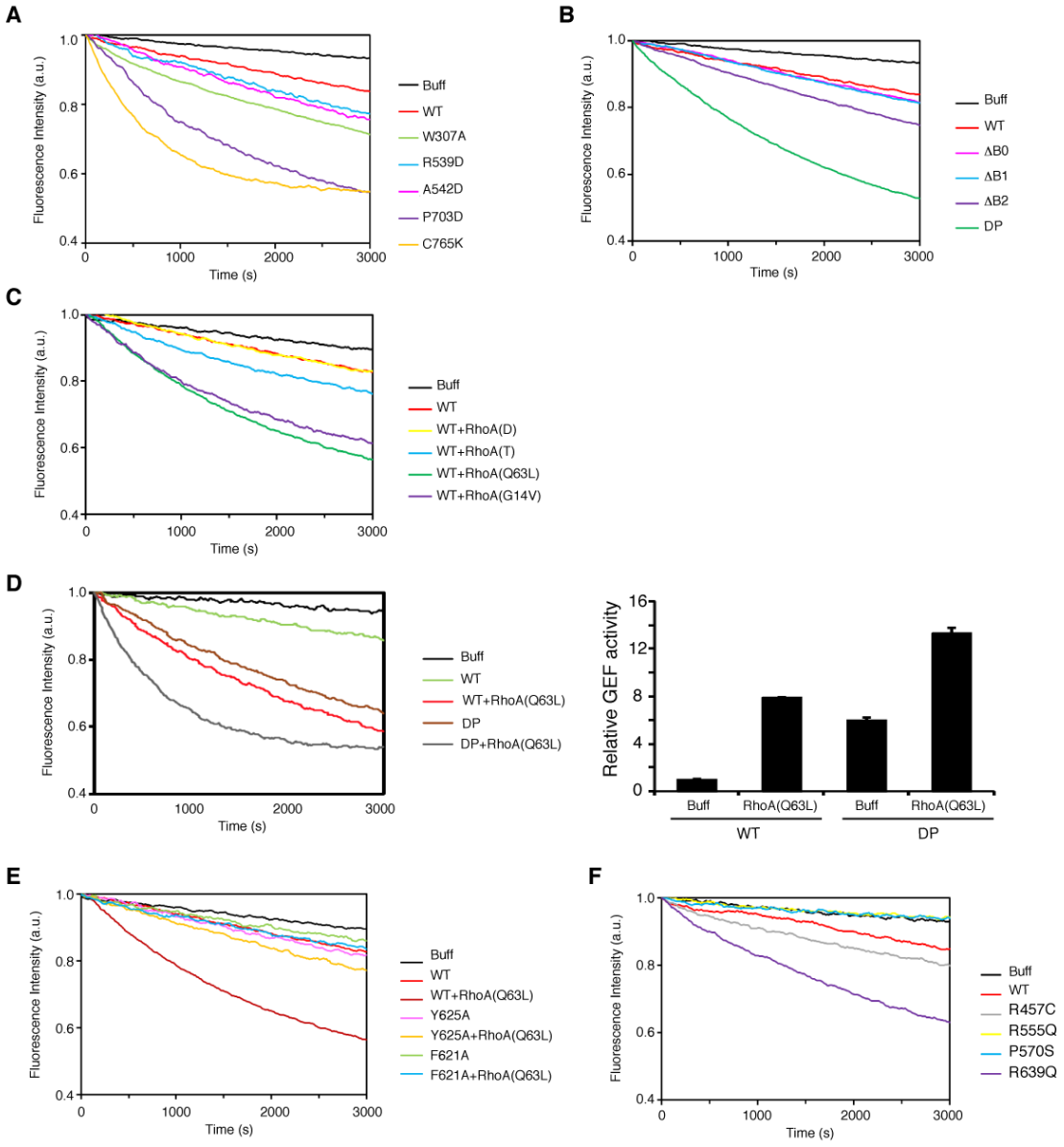

Fig. S4 GEF activity measurements of WT and varied mutants. (**A**) Point mutations at the inhibition interface. (**B**) Truncation of Ect2 to different boundaries. (**C**) WT protein in presence of RhoA in different states. (**D**) Activation of DP Ect2 by RhoA (Q63L). Quantitation of the activity shown on the right. (**E**) Point mutants at the allosteric activation interface. (**F**) Cancer-associated mutations.

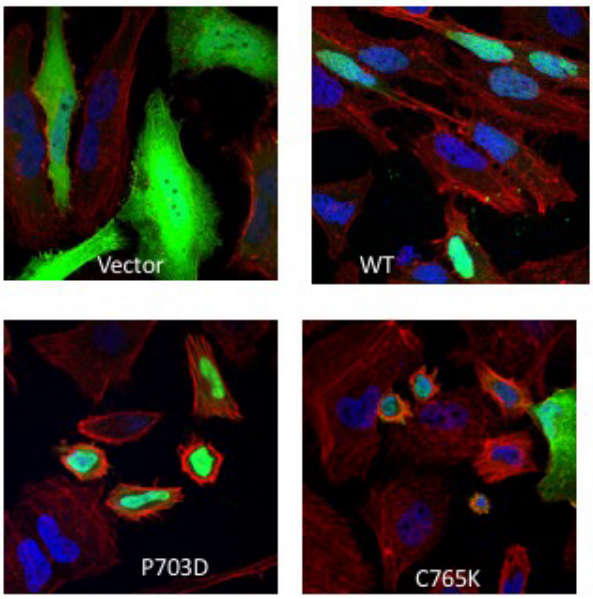

Fig. S5 Morphology of HeLa cells overexpressing WT and mutant Ect2. The experiments were conducted similarly as described in Fig. 3D.

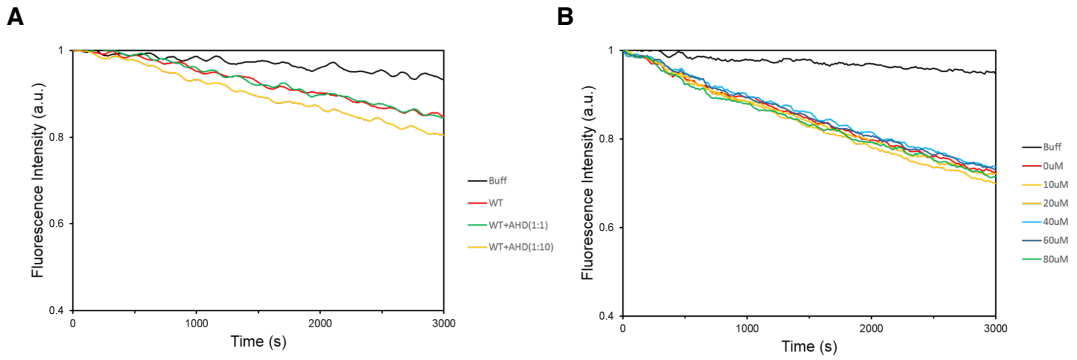

Fig. S6 GEF activity measurements of WT Ect2 in the presence of Anillin or a phosphorylated Cyk4 peptide. (**A**) Increasing molar ratios of the C-terminal Anillin-homology domain (residues 712-981) was added to WT Ect2 (2.5 μM). (**B**) Different concentrations of a phosphorylated Cyk4 peptide, S164P:DKTDES(p)LDWDSS, were used.

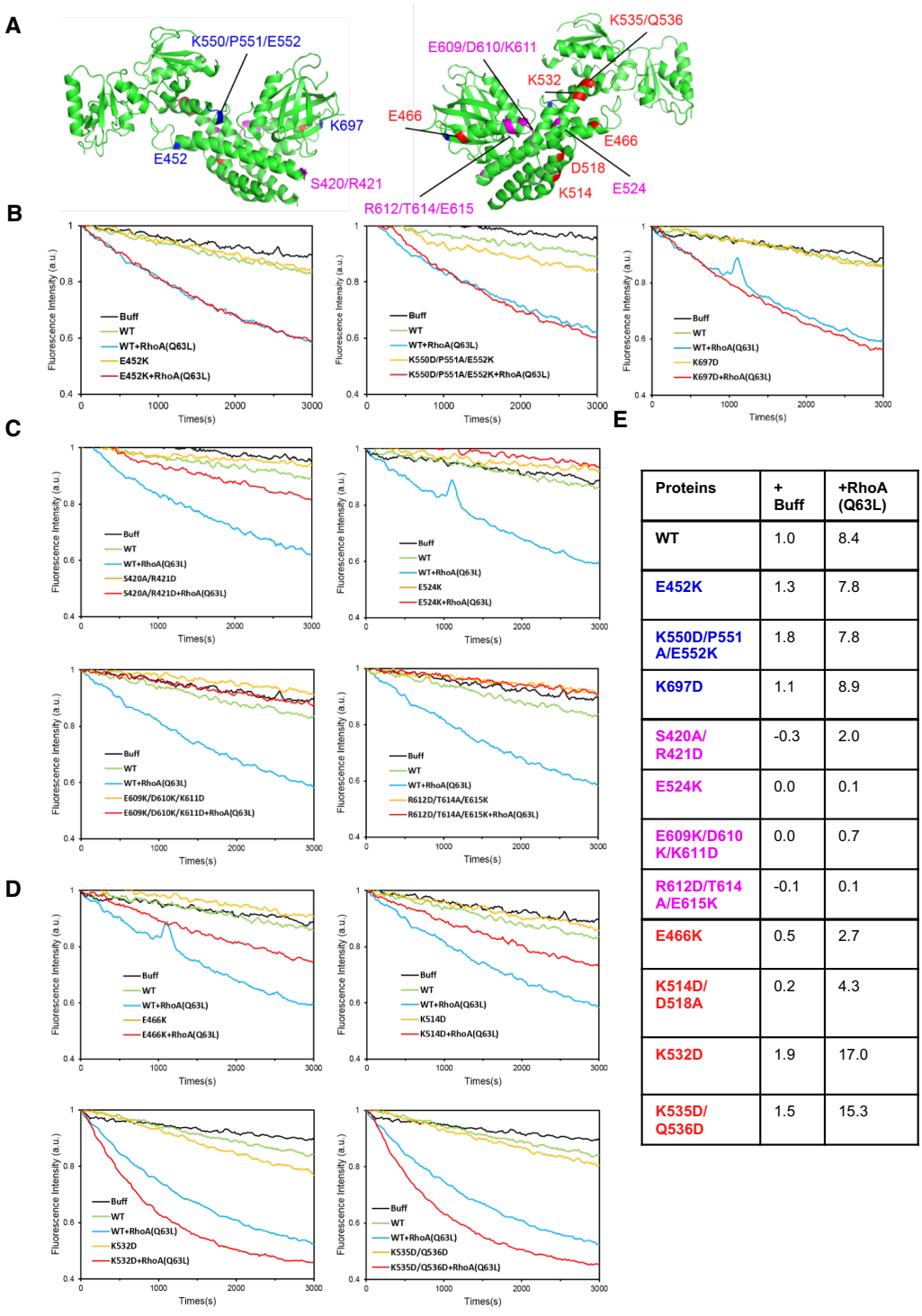

Proteins	+ Buff	+RhoA (Q63L)
WT	1.0	8.4
E452K	1.3	7.8
K550D/P551 A/E552K	1.8	7.8
K697D	1.1	8.9
S420A/ R421D	-0.3	2.0
E524K	0.0	0.1
E609K/D610 K/K611D	0.0	0.7
R612D/T614 A/E615K	-0.1	0.1
E466K	0.5	2.7
K514D/ D518A	0.2	4.3
K532D	1.9	17.0
K535D/ Q536D	1.5	15.3

Fig. S7 A series of Ect2 mutants failed the test for their ability to selectively compromise RhoA activation without perturbation of the basal GEF activity. (**A**) Mapping the mutants on the structure of Ect2. (**B**) Mutants (E452K, K550D/P551A/E552K, and K697D) showing no defect in either the basal activity or the RhoA-stimulating activity. (**C**) Mutants (S420A/ R421D, E524K,

E609K/D610K/K611D, and R612D/T614A/E615K) showing loss of the basal activity. (**D**) Mutants (E466K, K514D/D518A, K532D, and K535D/Q536D) showing no loss in the RhoA-stimulating activity. (**E**) Quantification of the relative GEF activities of the mutants.

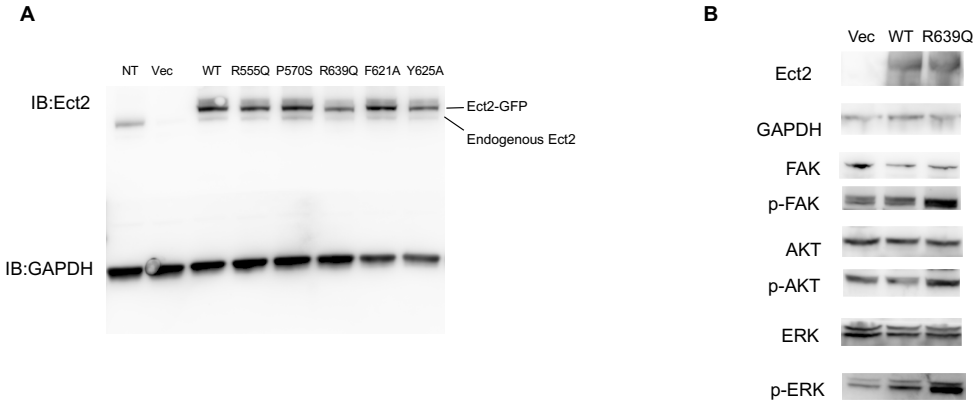

Fig. S8 Expression of various Ect2 constructs. (**A**) Ect2 expression levels of various constructs used in this study. NT, HeLa cells treated with negative control siRNA; Vec, cells with endogenous Ect2 knocked down and transfected with empty vector. (**B**) The R639Q mutant in A375 cells stimulated phosphorylation of Akt, ERK and FAK.

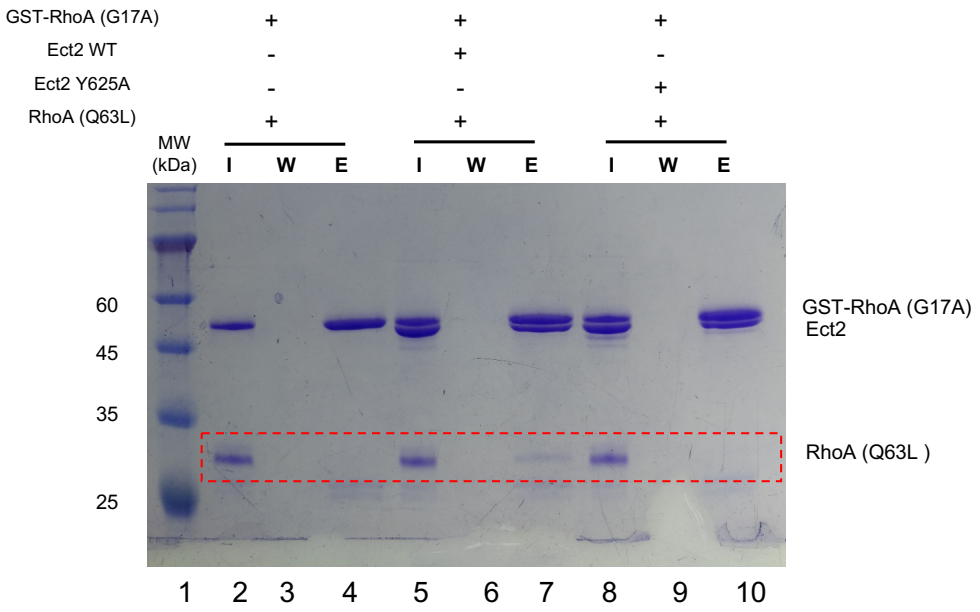

Fig. S9 GST-pulldown assays. GST-RhoA (G17A) pulled down RhoA (Q63L) in the presence of WT Ect2 (lane 7), but not in its absence (lane 3) or in the presence of the Y625A mutant (lane 10). I, input; W, wash; E, elute. Probably due to the interaction at not a particularly high affinity, the amount of RhoA (Q63L) pulled down is substoichiometric,

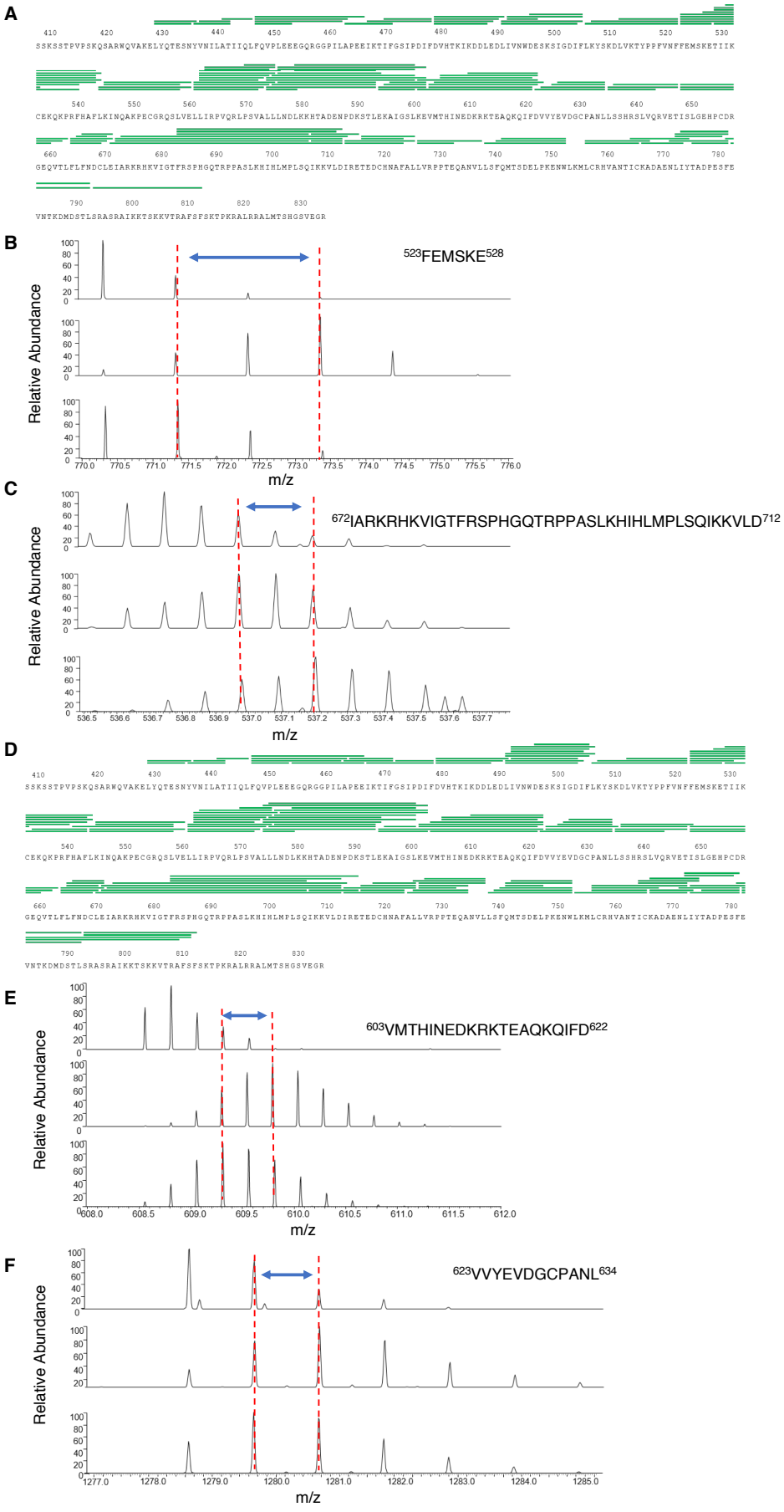
A
B
523FEMSKE528
Relative Abundance
m/z
C
672IARKRHKVIGTFRSPHGQTRPPASLKHIHLMPLSQIKKVLD712
Relative Abundance
m/z
D
E
603VMTHINEDKRKTEAQKQIFD622
Relative Abundance
m/z
F
623VVYEVDGCPANL634
Relative Abundance
m/z

Fig. S10 HDX-MS analyses of the model of two RhoA binding. (A) HDX-MS peptide coverage map of Ect2 (DP) in the presence of RhoA G17A. The green bars indicate detected peptides. The coverage is 89.2%. (**B-C**) Representative deuterium exchange mass spectra of Ect2 (DP) peptide fragments in the absence and presence of RhoA (G17A) . Top panel, undeuterated Ect2 (DP) sample; middle panel, Ect2 (DP) after 5 min in deuterated buffer; bottom panel, Ect2 (DP) in the presence of RhoA (G17A) after 5min in deuterated buffer. Dashed lines show the shift of the peaks. Peptide spanning residues 523-528 showed reduced exchange in the presence of RhoA (G17A) (B), whereas peptide spanning residues 672-712 displayed increased exchange (C). (**D**) HDX-MS peptide coverage map of Ect2 (DP) in presence of RhoA (G17A) and RhoA (Q63L). The coverages is 89.9%. (**E-F**) Representative deuterium exchange mass spectra of the Ect2 (DP)-RhoA (G17A) complex in the absence and presence of RhoA (Q63L). Peptides spanning residues 603-622 (E) and residues 623-634 (F) are shown here. Top panel, undeuterated Ect2 (DP)-RhoA (G17A) complex; middle panel, Ect2 (DP)-RhoA (G17A) complex after 5 min in deuterated buffer; bottom panel: Ect2 (DP)-RhoA (G17A) complex bound by RhoA (Q63L) after 5 min in deuterated buffer. Dashed lines show the shift of the peaks.

Table S1: SAXS data collection parameters and software employed for data analysis.

Data Collection Parameters	
Facilities and parameters	Settings and values
Beam line	12ID-B (APS, ANL)
Wavelength (Å)	0.8857
Detector	Pilatus 2M (SAXS)
q range ($Å^{-1}$)	0.005-0.89
Exposure time (s)	30-60
Concentration range (mg/ml)	0.75-3
Temperature (K)	298
Software Employed	
Primary Data Processing	Matlab/PRIMUS
P(r) Function	GNOM
SAXS Profile Computation	CRYSOL
Molecular Visualization	PyMol

Table S2 Fluorescence decay constant measured in the GEF activity assays.

Proteins	Rep. 1	Rep. 2	Rep. 3
Fig.2A			
buffer	5.34E-05	5.55E-05	4.49E-05
DH-PH	6.89E-04	7.87E-04	7.47E-04
WT	1.19E-04	1.23E-04	1.27E-04
ΔB0	1.51E-04	1.70E-04	1.83E-04
ΔB1	1.55E-04	1.50E-04	1.67E-04
ΔB2	2.37E-04	2.41E-04	2.57E-04
W307A	3.70E-04	3.06E-04	2.54E-04
R539D	1.83E-04	2.17E-04	1.97E-04
A542D	2.39E-04	3.23E-04	2.93E-04
P703D	7.01E-04	1.11E-03	1.02E-03
C765K	2.09E-03	1.62E-03	1.28E-03
Fig.3A			
buffer	1.24E-06	6.73E-05	7.16E-05
DH-PH	4.25E-04	4.01E-04	4.03E-04
WT	1.21E-04	1.08E-04	1.16E-04
RhoA(D)	1.36E-04	1.19E-04	1.36E-04
RhoA(T)	2.36E-04	2.21E-04	2.24E-04
RhoA(Q63L)	5.92E-04	6.08E-04	6.40E-04
RhoA(G14V)	3.88E-04	3.69E-04	3.87E-04
Fig.3A			
buffer	4.34E-05	4.73E-05	4.36E-05
DH-PH	3.13E-04	3.02E-04	2.92E-04
WT	1.21E-06	8.92E-05	9.09E-05
WT+RhoA(Q63L)	3.81E-04	3.80E-04	3.85E-04
Y625A	8.01E-05	7.81E-05	7.55E-05
Y625A+RhoA(Q63L)	1.08E-04	1.07E-04	1.15E-04
F621A	8.64E-05	8.28E-05	8.58E-05
F621A+RhoA(Q63L)	9.39E-05	9.90E-05	1.07E-04
Fig.5B			
buffer	4.54E-05	5.29E-05	3.88E-05
DH-PH	6.03E-04	4.84E-04	4.93E-04
WT	1.14E-04	9.28E-05	7.54E-05
R457C	1.39E-04	1.25E-04	1.43E-04
R555Q	3.05E-05	3.07E-05	4.17E-05
P570S	4.35E-05	2.96E-05	3.81E-05
R639Q	3.65E-04	3.03E-04	3.19E-04

Movie S1 | Knocking down endogenous Ect2 by siRNA resulted in cytokinesis failure, which could not be rescued by the empty vector.

Movie S2 | WT Ect2 rescued the cytokinesis failure caused by knocking down endogenous Ect2.

Movie S3 | F621A mutant Ect2 did not rescue the cytokinesis failure caused by knocking down endogenous Ect2.

Movie S4 | Y625A mutant Ect2 did not rescue the cytokinesis failure caused by knocking down endogenous Ect2.

Additional references:

1. Zou Y, *et al.* (2014) Crystal structure of triple-BRCT-domain of Ect2 and insights into the binding characteristics to CYK-4. *FEBS Lett.* 588(17):2911-2920.
2. Zhang D & Glotzer M (2015) The RhoGAP activity of CYK-4/MgcRacGAP functions non-canonically by promoting RhoA activation during cytokinesis. *Elife* 4.
3. Waterhouse A, *et al.* (2018) SWISS-MODEL: homology modelling of protein structures and complexes. *Nucleic Acids Res.* 46(W1):W296-W303.
4. Snyder JT, *et al.* (2002) Structural basis for the selective activation of Rho GTPases by Dbl exchange factors. *Nat. Struct. Biol.* 9(6):468-475.
5. Soisson SM, Nimnual AS, Uy M, Bar-Sagi D, & Kuriyan J (1998) Crystal structure of the Dbl and pleckstrin homology domains from the human Son of sevenless protein. *Cell* 95(2):259-268.
6. Ashkenazy H, *et al.* (2016) ConSurf 2016: an improved methodology to estimate and visualize evolutionary conservation in macromolecules. *Nucleic Acids Res.* 44(W1):W344-350.
7. Qu M, *et al.* (2013) Phosphorylation-dependent assembly and coordination of the DNA damage checkpoint apparatus by Rad4(TopBP1). *Mol. Cell* 51(6):723-736.
8. Lutz S, *et al.* (2007) Structure of Galphaq-p63RhoGEF-RhoA complex reveals a pathway for the activation of RhoA by GPCRs. *Science* 318(5858):1923-1927.